ACS APPLIED MATERIALS & INTERFACES

Research Article

Cite This: ACS Appl. Mater. Interfaces 2019, 11, 11645−11653

www.acsami.org

Unidirectional Real-Time Photoswitching of Diarylethene Molecular Monolayer Junctions with Multilayer Graphene Electrodes

Jeongmin Koo,[†,#] Yeonsik Jang,[†,#] León Martin,[‡,§] Dongku Kim,[§] Hyunhak Jeong,[†] Keehoon Kang,[†] Woocheol Lee,[†] Junwoo Kim,[†] Wang-Taek Hwang,[†] Dong Xiang,[∥] Elke Scheer,[§] Mikhail Kabdulov,[⊥] Thomas Huhn,[⊥] Fabian Pauly,*[,‡,§] and Takhee Lee*[,†]

[†]Department of Physics and Astronomy, and Institute of Applied Physics, Seoul National University, Seoul 08826, Korea

[‡]Okinawa Institute of Science and Technology Graduate University, Onna-son, Okinawa 904-0495, Japan

[§]Department of Physics and [⊥]Department of Chemistry, University of Konstanz, 78457 Konstanz, Germany

[∥]Tianjin Key Laboratory of Optoelectronic Sensor and Sensing Network Technology, College of Electronic Information and Optical Engineering, Nankai University, 300071 Tianjin, China

Supporting Information

ABSTRACT: We fabricate and characterize vertical molecular junctions consisting of self-assembled monolayers of diarylethene (DAE) contacted by a multilayer graphene (MLG) electrode on the top and gold on the bottom. The DAE molecular junctions show two stable electrical states, a closed state (high conductance) or an open state (low conductance), which are created upon illumination with UV or visible light, respectively. For the Au-DAE-MLG junction structure, we observe that the current levels between the two conductance states are separated by 2 orders of magnitude. However, in a real-time measurement, we observe only unidirectional switching behavior from the open to the closed state.

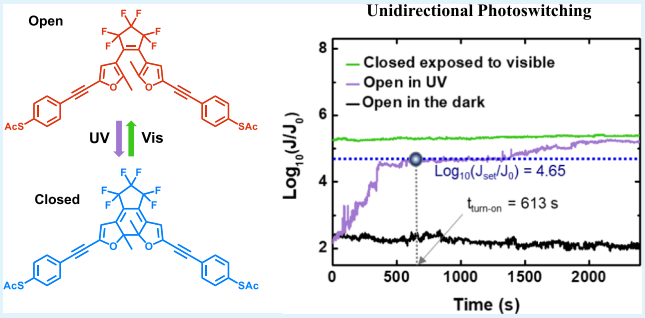

KEYWORDS: *molecular electronics, photoswitching, diarylethene, self-assembled monolayer, graphene electrode*

1. INTRODUCTION

To achieve the ultimate miniaturization of electronic devices, a wide range of studies in the field of molecular electronics has been carried out over the last decades. Important developments include utilization of functional molecules for realizing molecular wires, rectifiers, switches, transistors, and thermoelectric devices.[1−10] Among such developments, the molecular switch is a promising building block because of its potential as a memory device. Usually, a molecular switch consists of two stable isomers and undergoes a transition between them upon exposure to an external stimulus, such as light, heat, or an electric field.[11−13] In particular, light is useful for switching devices because of its addressability and compatibility with solid-state device structures. Therefore, the design of photochromic molecules is important for molecular switching devices. Diarylethenes (DAEs) form a class of photochromes with two different conductance states, that is, a high-conductance (closed; ON) and a low-conductance (open; OFF) state. In solution, DAEs can be converted between these two states by illumination with UV or visible light, respectively. This property makes them good candidates for photoswitching devices because of a large conductance difference between the two states and their response to light.[14−16]

As promising photoswitching molecules, DAEs have been utilized in various ways with the aim to demonstrate bidirectional switching in molecular devices. For an Au-DAE-Au junction, only unidirectional switching from the closed to the open state has been observed.[17] Subsequent theoretical studies have explained this nonreversibility of the DAE molecular junction by the strong coupling between the molecule and the metallic electrode, which leads to quenched molecular states.[18,19] On the other hand, unidirectional switching from the low- to the high-conductance state in Au-DAE-Au single-molecule junctions was obtained by modifying the side-arms and end-groups such that they form rigid conjugated molecular wires.[20] These molecules feature very high quantum yield for the ON switching reaction, but relatively low one for the OFF switching, explaining the inversed unidirectional switching. In addition, a similar single DAE molecule, bridged between carbon nanotubes[15] or graphene sheets,[21] showed unidirectional switching from the open to the closed state because strong molecule−electrode couplings between closed state DAE and graphene electrodes

Received: November 5, 2018
Accepted: March 1, 2019
Published: March 1, 2019

DOI: 10.1021/acsami.8b19372
ACS Appl. Mater. Interfaces 2019, 11, 11645−11653

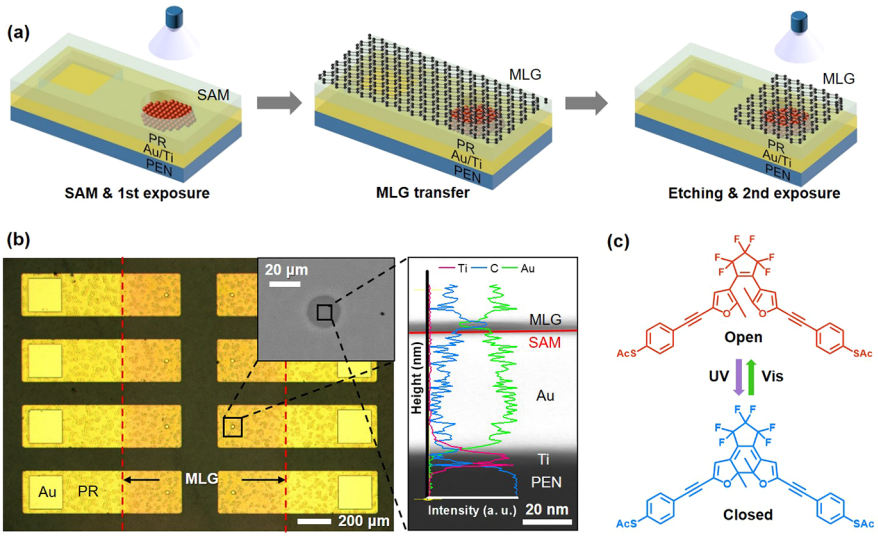

Figure 1. (a) Schematic representation of the fabrication process for the molecular junctions. (b) Optical (left), SEM (inset), and cross-sectional TEM (right) image of the fabricated molecular junctions. The TEM image is superimposed with an atomic composition profile measured by EDS. (c) Chemical structures of the DAE molecule in the open (top) and closed (bottom) states.

enabled the energy transfer from the photoexcited molecule to the extended π-electron system in the electrodes.[7,21] To overcome this unidirectional switching in DAE molecular junctions, various attempts were made. For example, through the introduction of a cross-conjugated system into the DAE molecule, namely metasubstituted phenyl end groups, the high-conductance state could be stabilized and thereby reversible switching in arrays of Au-DAE-Au junctions was demonstrated.[22] For DAE junctions with graphene electrodes, the unidirectional switching properties could be turned into bidirectional switching by adding alkane groups into both sides of the molecular backbone.[7] This series of studies demonstrates that the side-arms and end-groups, which provide the coupling between the molecule and the electrodes, play an important role in the switching characteristics because they control the energetic alignment between the Fermi level and the current-carrying molecular orbitals (MO) and the MOs' linewidth broadening.[20,23]

Molecular photoswitching devices have been developed beyond single-molecule junctions to realize large-area molecular junctions based on DAE molecules. Kronemeijer et al. demonstrated reliable bidirectional photoswitching for such large-area molecular junctions processed with self-assembled monolayers (SAMs) of DAEs, when poly(3,4-ethylenedioxythiophene):poly(styrene sulfonate) (PEDOT:PSS) was used as the top interlayer in addition to Au electrodes.[24] However, in our recent work on slightly modified DAE molecules, we found no optically induced switching, although the junction structure was the same as above.[16] This observation indicates that the mechanisms behind the photoswitching phenomenon in large-area molecular junctions still remain elusive.

We have previously reported the observation of bidirectional photoswitching behavior in DAE molecular junctions fabricated via self-assembly on an Au bottom electrode with a reduced graphene oxide (rGO) top electrode, which can withstand external mechanical stress.[25] In the present study, we employ MLG as the top electrode in the molecular junction, which shows a superior optical transmittance and higher conductance than that of the rGO electrode. At the same time, however, we find that the junction no longer exhibits the bidirectional switching behavior; instead, the device can only be switched from the OFF to the ON state, that is, from the open to the closed state of the employed 1,2-bis(2-methyl-5-(4-mercaptophenylethynyl)furan-3-yl)perfluorcyclopent-1-ene DAE. By performing a quantitative analysis in terms of the Landauer coherent transport model, we attribute the unidirectionality mainly to an increased electronic coupling between the closed state of the molecule and the MLG electrode as compared to the situation for rGO.

2. EXPERIMENTAL SECTION

2.1. Synthesis of MLG. The MLG film was synthesized by chemical vapor deposition (CVD) on catalytic metal surfaces.[26−31] Ni (300 nm)/Ti (20 nm) substrates purchased from Jinsol, Inc. were cleaned respectively in acetone, methanol, 2-propanol, and deionized (DI) water with an ultrasonicator for 10 min each. Then, the substrates were loaded into a CVD system (Teraleader Co., Korea) and preheated at 500 °C with a 200 sccm stream of Ar/H_2 at 800 Torr for ∼30 min to eliminate the oxidized layer on the Ni surface. Afterward, MLG films were grown under a gas flow of 15 sccm CH_4 and 20 sccm Ar/H_2 at 20 Torr for 5 min at 900 °C.

2.2. Molecular Junction Fabrication. Figure 1a shows a brief schematic diagram of the fabrication procedure used for the molecular junctions described in this study. We followed the well-established fabrication process that we have previously reported.[32,33] We chose poly(ethylene-2,6-naphthalate) (PEN) (Q83 purchased from Teijin DuPont Film Co., Ltd.) as the substrate material for the molecular junctions to enable operation even under mechanically flexible conditions (see Figure S5 in the Supporting Information). Au (50 nm)/Ti (5 nm) bottom electrodes were deposited onto the PEN substrates at a slow deposition rate of ∼0.2 Å/s using an electron beam evaporator. Next, a photoresist (PR) was spin-coated onto the surface, and circular holes with a radius of 10 μm were created on the PR film to expose the surface of the Au electrode by photolithography. The patterned samples were hard-baked at 190 °C for ∼2 h to enhance the chemical resistance to the SAM solution. For the SAM deposition, each sample was dipped into a diluted DAE solution (∼3 mM in ethanol solvent) for 24 h in a N_2-filled glove box with a few drops of ammonium hydroxide (NH_4OH) added into the solution, which is required to deprotect the acetyl group from the thiol end group. The molecular structure of the DAE under study is illustrated in Figure 1c. As described in detail in a previous paper,[34]

DOI: 10.1021/acsami.8b19372
ACS Appl. Mater. Interfaces 2019, 11, 11645−11653

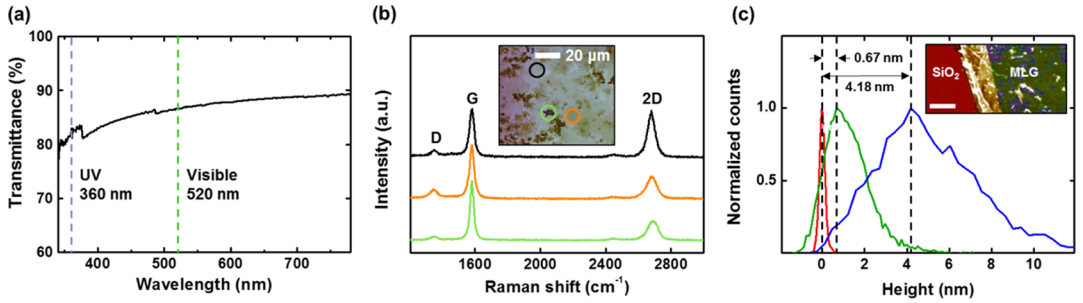

Figure 2. (a) Measured optical transmittance of a MLG film on a glass substrate. (b) Raman spectra for three different areas of a MLG film. (c) Topographic profile of a MLG film. The white scale bar in the inset image represents 4 μm.

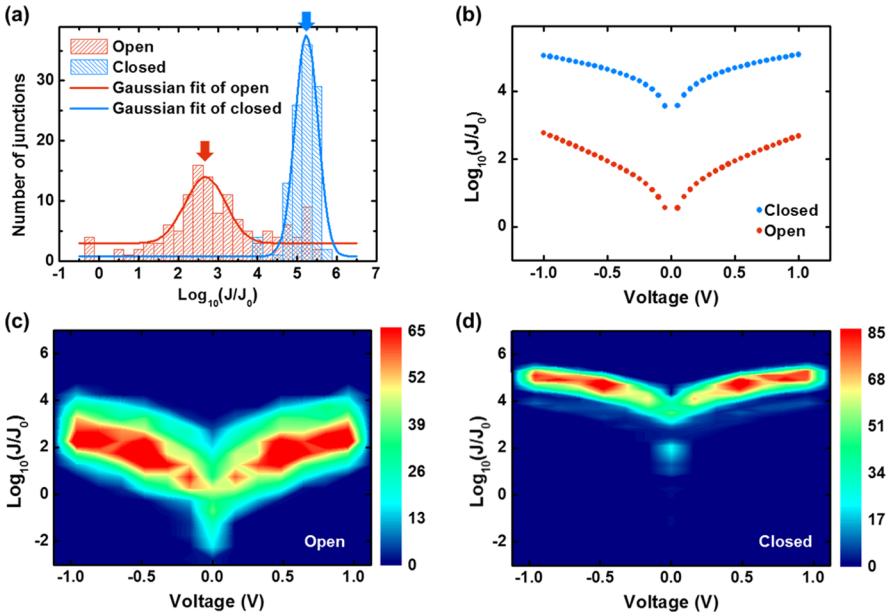

Figure 3. (a) Histogram of current-density values for all open- and closed-state molecular junctions measured at a bias of V = 1 V. (b) Representative logarithmic J–V curves for the closed and open state DAE molecular junctions. (c,d) Two-dimensional logarithmic J–V plots for intact molecular junctions in (c) open and (d) closed states. Here, J_0 = 1 A/cm^2 (see the text).

the DAE molecules are known to be attached via S–Au bonds to Au surfaces and form a somewhat disordered monolayer. Furthermore, X-ray photoelectron spectroscopy (XPS) and model calculations for DAE were presented by Kronemeijer et al.[24] In that paper, the experimentally estimated molecular layer thickness from the analysis of XPS data was ~2.0 nm for the closed state and ~2.4 nm for the open state. This result implies that the DAE in the closed state exhibits a more tilted off-normal angle than the open state. Also, this observation implies that the molecules are in a "standing" configuration with only one thiol bound to the Au electrode, instead of a "lying-down" one with both thiols bound to the metal. Afterward, we softly rinsed the samples with anhydrous ethanol and exposed each sample to 360 nm UV or 520 nm visible light to induce the closed or open state, respectively. Next, the MLG film was transferred to the molecular layer to make a contact through van der Waals interaction. The detailed procedure for preparing the transfer will be described in the following section. The unnecessary MLG part was removed via a shadow mask by means of an oxygen plasma treatment (under 10 sccm of O_2 gas at 50 W of power) to define each junction. Lastly, we once more exposed each sample to light (UV or visible) to ensure that the molecules remained in the desired state. The entire process after the SAM deposition was conducted in the dark to avoid undesirable effects caused by light exposure. Figure 1b shows the images of the fabricated molecular junctions obtained from optical microscopy, scanning electron microscopy (SEM), and cross-sectional transmission electron microscopy (TEM). From the atomic composition profile determined from energy-dispersive X-ray spectroscopy (EDS) along the cross section shown in Figure 1b, we could confirm that the C-rich part exists in the MLG and SAM layer between the surrounding Au parts. On the other hand, it was observed that the relative proportion of Au atoms decreased in these layers. This observation indicates that the MLG and SAM layers were well deposited and clearly distinguishable from the Au electrode. The Au peak at the top reflects an Au protection layer needed for the EDS measurement and deposited using a focused ion beam process. More details of the fabrication procedure for the molecular junctions are illustrated in Figure S1 of the Supporting Information.

2.3. Preparation of the MLG Top Electrode. The MLG film of the previous section is synthesized on Ni substrates. Subsequently, it is spin-coated with poly(methyl methacrylate) (PMMA, 950PMMA A5 from MicroChem Corp.) as a dummy layer. The Ni layer beneath the MLG film was etched by an iron(III) chloride ($FeCl_3$) aqueous solution. The floating MLG film, detached from the substrate, was rinsed with DI water more than three times to eliminate the adhered Fe and Ni ions. Then, the cleaned MLG film was placed onto the molecular layer as the top electrode of the molecular junction. After drying for a few hours to ensure good contact with the molecules, the PMMA layer was removed with acetone and isopropyl alcohol.

2.4. Electrical Characterization. The electrical characteristics of the molecular junctions were measured with a semiconductor parameter analyzer (Keithley 4200 SCS) and a probe station system (JANIS model ST-500) under ambient conditions.

DOI: 10.1021/acsami.8b19372
ACS Appl. Mater. Interfaces 2019, 11, 11645–11653

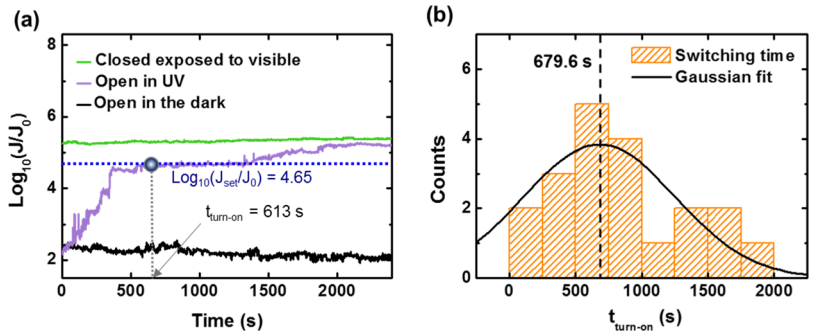

Figure 4. (a) Real-time measurement of the current density for each state with or without exposure to light at an applied bias voltage of V = 1 V. The switching time ($t_{turn\text{-}on}$) is indicated by an arrow. (b) Histogram for the measured switching time required to transition from the open to the closed state. The Gaussian fit to the histogram is shown by the solid line, and the average switching time is shown by the dashed line.

3. RESULTS AND DISCUSSION

As depicted in Figure 2, we have investigated the optical and morphological traits of the MLG film to confirm its suitability for use as the top electrode in Au-DAE-MLG junctions. Figure 2a presents the optical transmittance of the MLG film measured under light illumination over a wavelength range from 340 to 780 nm. As the MLG film shows a transmittance of more than 80% at both 360 and 520 nm, the material can be considered adequately transparent at the wavelengths at which the state of DAE can be transformed. The typical D, G, and 2D peaks of the MLG film in the Raman spectrum at energy shifts of 1350, 1580, and 2680 cm^{-1}, respectively, are shown in Figure 2b. The individual colored lines in this graph indicate the Raman peaks for the corresponding areas in the optical microscope (OM) image shown in the inset. The region marked by a black circle in the OM image has similar intensities for the G and 2D peaks in the Raman spectrum (black line). This indicates that the MLG film in that region is relatively thin and can be regarded as triple-layer graphene. On the other hand, the height of the 2D peaks is approximately half of those of the G peaks in the green and orange encircled regions in the OM image, and thus these areas are considered to be thicker multilayers.[35] Figure 2c shows the topographic profile of a MLG film transferred onto a SiO_2/Si substrate. Each colored line in the graph represents the area marked with the same color in the atomic force microscope image shown in the inset. The normalized count denotes the number of pixels for a certain height in each area divided by the maximum value of counts as obtained over all heights. This analysis shows that most of the area marked in green in the inset image has a thickness of 0.67 nm, which is similar to that of a monolayer of graphene, and that the small areas marked in blue have a thickness of 4.18 nm. When zooming in on the area of the green region, we find many multilayer features. Therefore, the results are in agreement with earlier reports that the MLG film, grown on a Ni substrate, is nonuniform, rather thick, and optically transparent.[26]

The current density−voltage (J−V) characteristics and their histograms for the DAE molecular junctions with an MLG top electrode are shown in Figure 3. The J−V data were obtained from the open and closed state junctions, fabricated separately. Figure 3a shows the histograms of the current density values for each state measured at 1 V from the entire set of working molecular junctions (131 molecular junctions in the open state and 111 molecular junctions in the closed state). Nonworking molecular junctions can be easily recognized as short-circuited or open-circuited and are excluded.[36] We defined the maximum of the Gaussian distribution, fitted to the histograms, as the representative current level of each state, as shown in Figure 3b. In Figure 3c,d, the two-dimensional J−V histograms are depicted as contour plots for all working open and closed state junctions, respectively. Although the variance of the current level in the open state is larger than that in the closed state, we find that the current levels of the two different states are separated by two orders of magnitude. This means that the molecular junctions with the MLG top electrode show distinct electrical properties in response to the light, similar to previous reports.[25]

Subsequently, we examined the phototransition properties of the DAE molecular junctions. Figure 4a shows real-time current density (J−t) measurements for three cases: open state in the dark (black line), open state exposed to 15 mW UV light (purple line), and closed state exposed to visible light (green line) with the same intensity as the UV light. All measurements were carried out under a constant voltage of 1 V, and the time on the x-axis of the graph was adjusted to start from the point when irradiation was initiated. The current level of the junction in the open state in the dark showed no changes, which suggests that the bias voltage applied to the molecular junction cannot induce the switching. In addition, for the case of the molecular junction prepared in the closed state, the switching behavior could not be observed when exposed to visible light. On the other hand, we observed a unidirectional real-time switching behavior from the open to the closed state under UV light illumination. We defined the switching time as the time to reach 90% of the average current value at 1 V in the closed state [$\log_{10}(J_{set}/J_0)$ = 4.65 with J_0 = 1 A/cm^2 and J_{set} chosen to be 90% of the average J value, as indicated by the blue arrow in Figure 3a]. The switching time of the representative molecular junction for the open state to transition to the closed state upon exposure to UV light was found to be 613 s (indicated as $t_{turn\text{-}on}$ in Figure 4a). The switching times obtained from 21 different molecular junctions (Figure S6, Supporting Information) were distributed as shown in Figure 4b. The average switching time for these 21 molecular junctions was determined to be about 680 s by performing a Gaussian fit to the statistical data, as shown in Figure 4b. Note that the photoswitching is intrinsically due to the UV-responsive reaction of the core of the DAE molecules. From irradiation experiments on a thiophene-derived DAE in solution, the irreversible formation of a nonphotoactive byproduct is known.[37] Such process could reduce the number of available fully functional molecular switches somewhat, but it would not render the whole device nonfunctional. However, during

DOI: 10.1021/acsami.8b19372
ACS Appl. Mater. Interfaces 2019, 11, 11645−11653

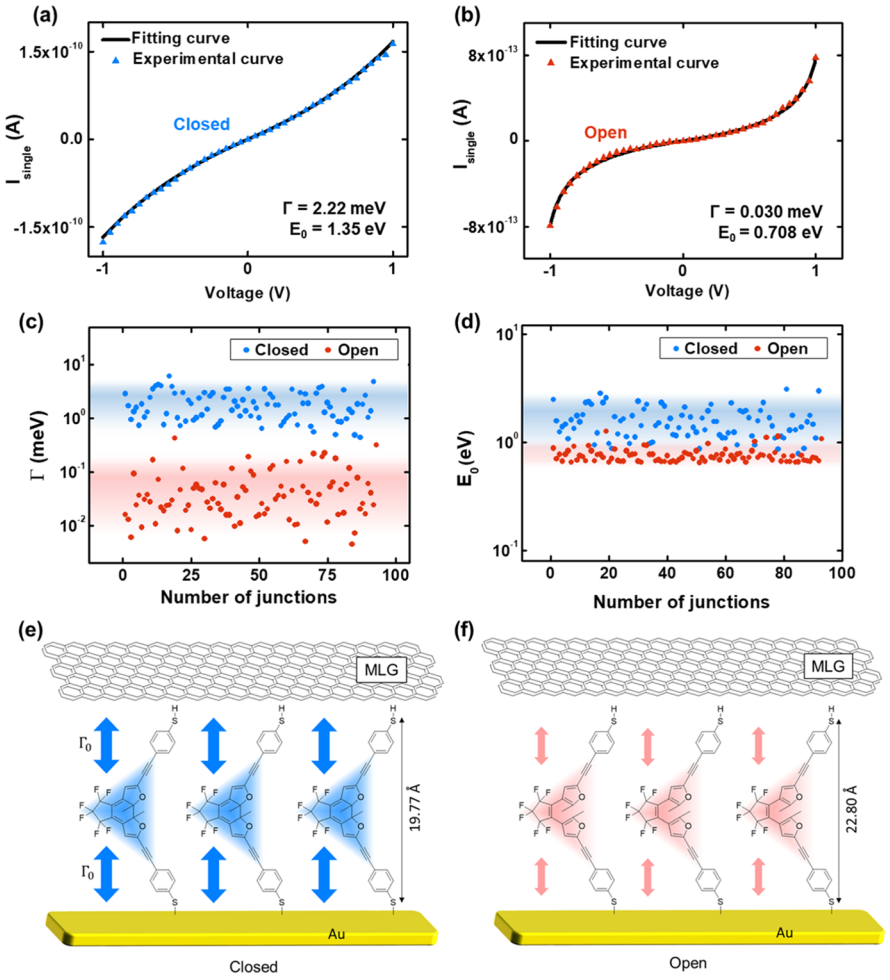

Figure 5. (a,b) A representative I_{single}–V curve measured for the (a) closed and (b) open state, with the fitting curve (shown as a solid line) calculated based on the Landauer formula. The corresponding coupling and level alignment values used in the fits are listed at the bottom right of each graph. (c,d) Scatter point plots for (c) Γ and (d) E_0 values for intact molecular junctions in the closed and open state. The shaded regions represent areas where the data points deviate by no more than 60% from the averages. Here, Γ values for the closed and open states are clearly separated from each other, whereas they mix for E_0. (e,f) Schematic illustration of junction structures for the (e) closed and (f) open state. The coupling strength between molecules and the electrodes, Γ, is indicated by the size of the arrow.

irradiation of our furan-bearing DAEs in solution, a similar fatigue mechanism was never observed. Also, we fabricated an empty junction that showed no change in its I–V characteristics upon UV irradiation (see Figure S3).

To gain a better understanding of the charge transport through the molecular junctions and to investigate the unidirectional switching behavior, we apply the Landauer formalism.[38] We approximate the current through an equivalent single-molecule junction as

$$I_{single} = \frac{c}{NA} I_{exp} = \frac{2e}{h} \int_{-\infty}^{\infty} T(E)[f_1(E) - f_2(E)]dE \quad (1)$$

In eq 1, $f_X(E) = (1 + \exp((E - \mu_X)/k_BT))^{-1}$ is the Fermi–Dirac distribution function, where μ_X is the chemical potential of the electrode, X = top or bottom, and $T(E)$ is the transmission function with a Lorentzian shape around the MO n described as

$$T(E) = \sum_n \frac{4\Gamma_{n,top}\Gamma_{n,bottom}}{[\Gamma_n^2 + (E - E_n)^2]} \quad (2)$$

Here, $\Gamma_{n,X}$ indicates the electronic coupling strength of the MO n to the respective electrode X, and $\Gamma_n = \Gamma_{n,top} + \Gamma_{n,bottom}$ defines the total linewidth broadening. Counting all energies from the Fermi energy, E_F, as the reference, E_n is the difference between the eigenenergy of the MO and the Fermi energy of the electrodes $\mu_X \approx E_F$.

As our system consists of many molecules, we calculate the current per molecule, I_{single}, by dividing the experimentally measured current, I_{exp}, by the number of molecules, NA, in the junction. Here, we choose the coverage, N, as 4.4×10^{14} and 5.4×10^{14} cm^{-2} for the closed-state and open-state DAE, respectively.[24] The reason why the packing density of the closed state is lower than that of the open state is because the energetically most favorable packing and tilt angle (i.e., the optimized molecular conformations that minimize the free energy) are different for the closed state and the open state.[24] The contact area, A, of the molecular junctions is estimated to be equal to the geometric hole size of 314 μm^2. Furthermore, we multiplied the current by a phenomenological factor c = 3000 because the current per molecule in SAMs has been found to be about 3000 times lower than that in a single-molecule junction in the case of a conjugated molecular wire.[39] This effect is attributed to the fact that SAMs are more effectively screening the external electric field and provide

DOI: 10.1021/acsami.8b19372
ACS Appl. Mater. Interfaces 2019, 11, 11645–11653

more paths for molecular heat dissipation as compared to single-molecule junctions. These factors facilitate the tunneling through a single-molecule junction as compared to the SAM system. Finally, because the number of molecules that make electrical contact with both electrodes in large-scale molecular junctions is only a fraction of the total number of molecules, per molecule the contact is less conductive than a single-molecule junction.[40]

Let us point out that we expect various defects in our experimental devices that cannot be controlled perfectly. For example, polymer residues, ripples, cracks, or voids on or in the CVD-grown MLG film will influence the effective contact area with the SAM.[41,42] Similarly, defects at the bottom electrode resulting from grain boundaries or PR residues may cause an irregular arrangement of molecules. Consequently, the actual contact area will be altered and distances between the molecules and electrodes will vary.[43,44] Considering these factors, the contact area and the distance between the SAM and the MLG can neither be accurately predicted nor measured.

To simplify the analysis of I_{single}, we introduce the following assumptions: (i) The contribution from a single MO $n = 0$ determines the current.[21,38] (ii) As the experimental $J-V$ characteristics are almost symmetric with regard to bias polarity, we assume that the coupling strength is symmetric, that is, $\Gamma = \Gamma_{0,top} + \Gamma_{0,bottom}$ and $\Gamma_{0,top} = \Gamma_{0,bottom}$.[45] (iii) The energy level E_0 of the SAM system is fixed, when a bias voltage is applied between the two electrodes.[38,45,46] By adopting these assumptions, eq 2 reduces to

$$T(E) = \frac{\Gamma^2}{[\Gamma^2 + (E - E_0)^2]} \quad (3)$$

where the charge injection barrier is given as $E_0 = E_{HOMO} - E_F$ or $E_0 = E_{LUMO} - E_F$ with E_{HOMO} and E_{LUMO} being the energy levels of the highest occupied molecular orbital (HOMO) and the lowest unoccupied molecular orbital (LUMO), respectively.

Let us note that with all these approximations, we use a very simple model to analyze the charge transport through the complex Au-DAE-MLG systems. Indeed, the symmetric single-level model appears to be oversimplified, given that junctions are structurally asymmetric. Thus, we expect that the DAE molecules exhibit a weak physical contact to MLG and a strong covalent bond to Au, making it necessary to distinguish between the two couplings, $\Gamma_{0,bottom}$ and $\Gamma_{0,top}$. However, the couplings also significantly depend on the intramolecular coupling strength between the central part of the molecule and the contact groups at the ends.[47] Indeed, Nijhuis and collaborators showed that both $J-V$ curves as well as $\Gamma_{0,bottom}$ and $\Gamma_{0,top}$ are almost symmetric for ferrocenyl-based molecules between one covalently bound and one physisorbed contact, when the ferrocenyl unit was located at the center of the molecule.[48] We, therefore, hope that the effective parameters Γ and E_0, extracted from the single-level model, yield meaningful trends. Let us also point out that only the absolute value of E_0, that is $|E_0|$, can be determined from current−voltage characteristics. To simplify the notation, we will omit the symbol for the absolute value in the following, and assume that $E_0 \geq 0$.

As described in a previous publication,[38] we have numerically fitted experimental $I_{single}-V$ curves to estimate Γ and E_0 values by adopting the Levenberg−Marquardt algorithm. Figure 5a,b show representative $I_{single}-V$ curves and the corresponding fits for the closed and open states. The fits reproduce the measurements well with minimal variation over the whole voltage range. In addition, we conducted the fitting for 91 closed-state and 84 open-state molecular junctions, and then extracted Γ and E_0 values for all junctions. All Γ and E_0 values determined are presented in the scatter plot in Figure 5c,d. More experimental $I_{single}-V$ characteristics and the corresponding fits can be found in Figure S7 in the Supporting Information. By averaging these distributions, the effective coupling strength, Γ, for closed and open states was determined to be 1.93 ± 0.12 and 0.0572 ± 0.0072 meV, respectively, and the corresponding charge injection barrier, E_0, for closed and open states was extracted to be 1.560 ± 0.054 and 0.756 ± 0.012 meV, respectively, as summarized in Table 1. Figure 5e,f show schematic illustrations of junction structures for closed- and open-state molecular junctions, where we have visualized the coupling strength, Γ, between the molecule and the electrodes by arrows of different size.

Table 1. Charge Injection Barrier (E_0) and Coupling Constant (Γ) as Extracted from a Set of $I_{single}-V$ Curves by Using the Landauer Formula

		Γ (meV)	E_0 (eV)
Au-DAE-MLG	closed	1.93 ± 0.12	1.560 ± 0.054
	open	0.0572 ± 0.0072	0.756 ± 0.012
Au-DAE-rGO	closed	0.462 ± 0.039	2.19 ± 0.18
	open	0.250 ± 0.040	2.72 ± 0.38

Note that the level alignment, E_0, shows a complex behavior opposite to the naive expectation that E_0 in the open state would be higher than for the closed state. This expectation is based on the fact that the electronic gap between the HOMO and the LUMO in an isolated DAE molecule is larger in the open state than in the closed one.

Calculations using various levels of ab initio electronic structure theory are summarized in Table 2. They have been carried out with the help of the program package TURBOMOLE.[49] As a first method, we have chosen density functional theory (DFT) together with PBE[50−52] as the exchange−correlation functional. Because the DFT typically underestimates quasiparticle gaps substantially by some eVs,[53] we have computed them also with ΔSCF,[53] G_0W_0,[54] and eigenvalue self-consistent GW (evGW).[55] All of these calculations show that the HOMO−LUMO gap of DAE

Table 2. Energies of HOMO and LUMO States in Open and Closed Configurations of the Isolated Molecules in Vacuum and the Resulting Electronic Gap

method	HOMO (eV)	LUMO (eV)	gap (eV)
	Closed		
DFT (PBE)	−4.57	−3.50	1.07
G_0W_0	−6.00	−0.40	5.60
evGW	−6.17	−1.97	4.20
ΔSCF	−6.02	−2.13	3.89
	Open		
DFT (PBE)	−5.03	−2.74	2.29
G_0W_0	−6.76	−1.01	5.75
evGW	−7.07	−0.46	6.61
ΔSCF	−6.32	−1.27	5.05

DOI: 10.1021/acsami.8b19372
ACS Appl. Mater. Interfaces 2019, 11, 11645−11653

decreases when being switched from the open to the closed state. This confirms the assertion made in the previous paragraph and matches well with the picture of more delocalized electrons in the closed state. Indeed, both HOMO and LUMO wavefunctions in the closed state spread more strongly over the hole molecule than in the open one, as is visible in Figure 6.

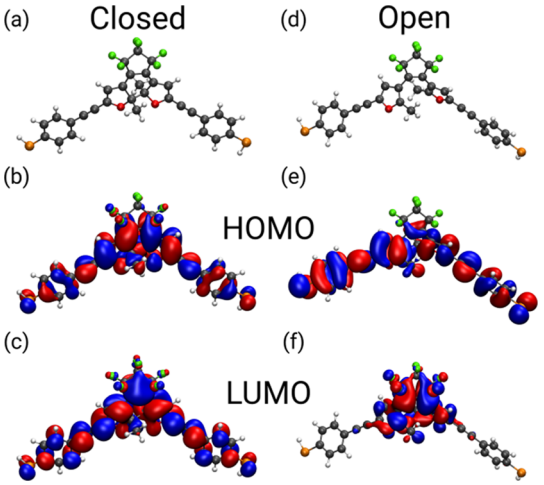

Figure 6. (a) Equilibrium geometry of the DAE molecule in the gas phase in its closed state, and corresponding (b) HOMO and (c) LUMO wavefunctions. (d–f) The same for the open state. The results are obtained from DFT-PBE calculations.

It is also apparent from the expression for the transmission in eq 3 that the difference in Γ values between closed and open states determines the magnitude of current rather than the difference in E_0 values. In particular, it is notable that the effective value of Γ in the closed state is more than 30 times larger than that of the open state, whereas E_0 differs only by a factor of around 2. Thus, the Γ values explain why the closed state is more conductive than the open one.

In addition to a previous explanation that the small quantum yield of the ring opening reaction reduces the switching rate,[20] the relatively strong coupling between DAE and MLG electrodes in the closed state may also cause the unidirectional switching. It is possible that the strong interaction between the closed state of the DAE molecules and the electrode can quench the photoexcited closed state, effectively disturbing the switching process and eventually preventing the transition to the open state.[17,56,57]

We also applied the same method to analyze the measurement data for Au-DAE-rGO junctions (Figure S8, Supporting Information) reported in our previous work.[25] In Figures S8a,b, representative fitting results are shown for closed and open states, both of which were well-fitted. The averaged fitting results, obtained from 10 Au-DAE-rGO junctions, are given in Table 1. The extracted Γ values for closed and open states were calculated as 0.462 ± 0.039 and 0.250 ± 0.040 meV, respectively, both of which are roughly one order lower than the value obtained for the closed state in Au-DAE-MLG junctions. The effective E_0 values for the closed and open states were found to be 2.19 ± 0.18 and 2.72 ± 0.38 meV, respectively. As depicted in Figure S8c, the distribution of Γ values for both states in the Au-DAE-rGO junctions is in a similar range within one order, in contrast to the Au-DAE-MLG junctions, which showed a significant difference in electronic couplings between closed and open states. Level alignments, E_0, between open and closed junctions in Figure S8d practically do not differ. This result corroborates that bidirectional switching in Au-DAE-rGO junctions correlates well with similar and small Γ values for both closed and open states.

The HOMO–LUMO gaps determined with ΔSCF, G_0W_0, and evGW in Table 1 are expected to be more reliable than those of DFT,[53] and we find, indeed, that they are much larger than the predictions of DFT. Let us point out that the quasiparticle electronic gap values can provide bounds for the level alignment E_0, used in the fits with the single-level model. In particular, it should be less than half of the gap size, $E_0 \leq \Delta/2$, because screening effects inside the junctions due to the presence of the electrodes and other molecules are expected to reduce the effective electronic gap. Although the bandgap values obtained from ΔSCF, G_0W_0, and evGW are compatible with the experimental values for E_0 from Au-DAE-MLG and Au-DAE-rGO junctions in open and closed states, DFT clearly violates the approximate relation, $E_0 \leq \Delta/2$.

The different tendency of the Γ values in the Au-DAE-MLG junctions compared to those in the Au-DAE-rGO junctions can reasonably explain why the former junctions show unidirectional switching, whereas the latter exhibit bidirectional switching. Our analysis reveals that the interaction between the molecules and the electrodes is important not only for the overall current level but also for the directionality of the switching behavior. We conclude that the interaction between the DAE molecules and different electrode materials can lead to drastically different device characteristics.

4. CONCLUSIONS

In summary, we fabricated and characterized DAE photoswitching molecular junctions using Au bottom and MLG top electrodes. We found clearly distinguishable electrical properties for the molecular junctions between closed and open states with average current levels differing by two orders of magnitude. At the same time, we found in real-time measurements that the junctions exhibited a unidirectional switching behavior from the open to the closed state. To better understand the unidirectionality, we extracted electronic coupling and level alignment parameters, Γ and E_0, by fitting experimental J–V curves with the Landauer formula. The calculated Γ value for the Au-DAE-MLG junctions in the closed state was significantly larger than in the open state. A comparison with previously measured Au-DAE-rGO junctions, which show bidirectional switching, revealed that the electronic couplings Γ correlate well with the photoswitching behavior and not the level alignment. By relating the electronic measurements with photoswitching device characteristics, we thus attribute the inability to switch to the open state to the strong coupling between DAE and the MLG electrode in the closed state, together with the low quantum yield of the opening reaction. Our study suggests that the electronic coupling between molecules and electrodes plays a significant role for any molecular photoswitching device.

■ ASSOCIATED CONTENT

Supporting Information

The Supporting Information is available free of charge on the ACS Publications website at DOI: 10.1021/acsami.8b19372.

DOI: 10.1021/acsami.8b19372
ACS Appl. Mater. Interfaces 2019, 11, 11645–11653

Detailed device fabrication procedure, stability of the molecular junctions, real-time measurement of switching, additional electrical characteristics and details on theoretical calculations for the electronic structure of gas-phase molecules are provided (PDF)

AUTHOR INFORMATION

Corresponding Authors

*E-mail: fabian.pauly@oist.jp (F.P.).
*E-mail: tlee@snu.ac.kr (T.L.).

ORCID

Dong Xiang: 0000-0002-5632-6355
Fabian Pauly: 0000-0001-8017-2379
Takhee Lee: 0000-0001-5988-5219

Author Contributions

#J.K. and Y.J. contributed equally.

Notes

The authors declare no competing financial interest.

ACKNOWLEDGMENTS

The authors appreciate financial support from the National Creative Research Laboratory program (grant no. 2012026372) through the National Research Foundation of Korea funded by the Korean Ministry of Science and ICT. L.M., M.K., T.H., E.S., and F.P. gratefully acknowledge funding through the Collaborative Research Center (SFB) 767 of the Deutsche Forschungsgemeinschaft (DFG, German Research Foundation). Part of the numerical modeling was performed using the computational resources of the bwHPC program, namely the bwUniCluster and the JUSTUS HPC facility.

REFERENCES

(1) Bumm, L. A.; Arnold, J. J.; Cygan, M. T.; Dunbar, T. D.; Burgin, T. P.; Jones, L.; Allara, D. L.; Tour, J. M.; Weiss, P. S. Are Single Molecular Wires Conducting? *Science* **1996**, *271*, 1705−1707.

(2) Wold, D. J.; Haag, R.; Rampi, M. A.; Frisbie, C. D. Distance Dependence of Electron Tunneling through Self-Assembled Monolayers Measured by Conducting Probe Atomic Force Microscopy: Unsaturated versus Saturated Molecular Junctions. *J. Phys. Chem. B* **2002**, *106*, 2813−2816.

(3) Tanaka, T.; Osuka, A. Conjugated Porphyrin Arrays: Synthesis, Properties and Applications for Functional Materials. *Chem. Soc. Rev.* **2015**, *44*, 943−969.

(4) Aviram, A.; Ratner, M. A. Molecular Rectifiers. *Chem. Phys. Lett.* **1974**, *29*, 277−283.

(5) Chen, X.; Roemer, M.; Yuan, L.; Du, W.; Thompson, D.; del Barco, E.; Nijhuis, C. A. Molecular Diodes with Rectification Ratios Exceeding 10^5 driven by Electrostatic Interactions. *Nat. Nanotechnol.* **2017**, *12*, 797−803.

(6) Osorio, E. A.; Moth-Poulsen, K.; van der Zant, H. S. J.; Paaske, J.; Hedegård, P.; Flensberg, K.; Bendix, J.; Bjørnholm, T. Electrical Manipulation of Spin States in a Single Electrostatically Gated Transition-Metal Complex. *Nano Lett.* **2009**, *10*, 105−110.

(7) Jia, C.; Migliore, A.; Xin, N.; Huang, S.; Wang, J.; Yang, Q.; Wang, S.; Chen, H.; Wang, D.; Feng, B.; Liu, Z.; Zhang, G.; Qu, D.-H.; Tian, H.; Ratner, M. A.; Xu, H. Q.; Nitzan, A.; Guo, X. Covalently Bonded Single-Molecule Junctions with Stable and Reversible Photoswitched Conductivity. *Science* **2016**, *352*, 1443−1445.

(8) Song, H.; Kim, Y.; Jang, Y. H.; Jeong, H.; Reed, M. A.; Lee, T. Observation of Molecular Orbital Gating. *Nature* **2009**, *462*, 1039−1043.

(9) Capozzi, B.; Chen, Q.; Darancet, P.; Kotiuga, M.; Buzzeo, M.; Neaton, J. B.; Nuckolls, C.; Venkataraman, L. Tunable Charge Transport in Single-Molecule Junctions via Electrolytic Gating. *Nano Lett.* **2014**, *14*, 1400−1404.

(10) Cui, L.; Miao, R.; Wang, K.; Thompson, D.; Zotti, L. A.; Cuevas, J. C.; Meyhofer, E.; Reddy, P. Peltier Cooling in Molecular Junctions. *Nat. Nanotechnol.* **2018**, *13*, 122−127.

(11) Seo, S.; Min, M.; Lee, S. M.; Lee, H. Photo-Switchable Molecular Monolayer Anchored between Highly Transparent and Flexible Graphene Electrodes. *Nat. Commun.* **2013**, *4*, 1920.

(12) Hagen, S.; Leyssner, F.; Nandi, D.; Wolf, M.; Tegeder, P. Reversible switching of tetra-tert-butyl-azobenzene on a Au(111) surface induced by light and thermal activation. *Chem. Phys. Lett.* **2007**, *444*, 85−90.

(13) Alemani, M.; Peters, M. V.; Hecht, S.; Rieder, K.-H.; Moresco, F.; Grill, L. Electric Field-Induced Isomerization of Azobenzene by STM. *J. Am. Chem. Soc.* **2006**, *128*, 14446−14447.

(14) Irie, M.; Kobatake, S.; Horichi, M. Reversible Surface Morphology Changes of a Photochromic Diarylethene Single Crystal by Photoirradiation. *Science* **2001**, *291*, 1769−1772.

(15) Whalley, A. C.; Steigerwald, M. L.; Guo, X.; Nuckolls, C. Reversible Switching in Molecular Electronic Devices. *J. Am. Chem. Soc.* **2007**, *129*, 12590−12591.

(16) Kim, D.; Jeong, H.; Lee, H.; Hwang, W.-T.; Wolf, J.; Scheer, E.; Huhn, T.; Jeong, H.; Lee, T. Flexible Molecular-Scale Electronic Devices composed of Diarylethene Photoswitching Molecules. *Adv. Mater.* **2014**, *26*, 3968−3973.

(17) Dulic, D.; van der Molen, S. J.; Kudernac, T.; Jonkman, H. T.; de Jong, J. J.; Bowden, T. N.; van Esch, J.; Feringa, B. L.; van Wees, B. J. One-Way Optoelectronic Switching of Photochromic Molecules on Gold. *Phys. Rev. Lett.* **2003**, *91*, 207402.

(18) Zhuang, M.; Ernzerhof, M. Reversibility and Transport Properties of Dithienylethene Photoswitches. *J. Chem. Phys.* **2009**, *130*, 114704.

(19) Zhuang, M.; Ernzerhof, M. Mechanism of a Molecular Electronic Photoswitch. *Phys. Rev. B: Condens. Matter Mater. Phys.* **2005**, *72*, 073104.

(20) Sendler, T.; Luka-Guth, K.; Wieser, M.; Lokamani, J.; Wolf, J.; Helm, M.; Gemming, S.; Kerbusch, J.; Scheer, E.; Huhn, T.; Erbe, A. Light-Induced Switching of Tunable Single-Molecule Junctions. *Adv. Sci.* **2015**, *2*, 1500017.

(21) Jia, C.; Wang, J.; Yao, C.; Cao, Y.; Zhong, Y.; Liu, Z.; Liu, Z.; Guo, X. Conductance Switching and Mechanisms in Single-Molecule Junctions. *Angew. Chem., Int. Ed.* **2013**, *52*, 8666−8670.

(22) van der Molen, S. J.; Liao, J.; Kudernac, T.; Agustsson, J. S.; Bernard, L.; Calame, M.; van Wees, B. J.; Feringa, B. L.; Schönenberger, C. Light-Controlled Conductance Switching of Ordered Metal-Molecule-Metal Devices. *Nano Lett.* **2008**, *9*, 76−80.

(23) Zotti, L. A.; Kirchner, T.; Cuevas, J.-C.; Pauly, F.; Huhn, T.; Scheer, E.; Erbe, A. Revealing the Role of Anchoring Groups in the Electrical Conduction Through Single-Molecule Junctions. *Small* **2010**, *6*, 1529−1535.

(24) Kronemeijer, A. J.; Akkerman, H. B.; Kudernac, T.; van Wees, B. J.; Feringa, B. L.; Blom, P. W. M.; de Boer, B. Reversible Conductance Switching in Molecular Devices. *Adv. Mater.* **2008**, *20*, 1467−1473.

(25) Kim, D.; Jeong, H.; Hwang, W.-T.; Jang, Y.; Sysoiev, D.; Scheer, E.; Huhn, T.; Min, M.; Lee, H.; Lee, T. Reversible Switching Phenomenon in Diarylethene Molecular Devices with Reduced Graphene Oxide Electrodes on Flexible Substrates. *Adv. Funct. Mater.* **2015**, *25*, 5918−5923.

(26) Reina, A.; Jia, X.; Ho, J.; Nezich, D.; Son, H.; Bulovic, V.; Dresselhaus, M. S.; Kong, J. Large Area, Few-Layer Graphene Films on Arbitrary Substrates by Chemical Vapor Deposition. *Nano Lett.* **2008**, *9*, 30−35.

(27) Chae, S. J.; Güneş, F.; Kim, K. K.; Kim, E. S.; Han, G. H.; Kim, S. M.; Shin, H.-J.; Yoon, S.-M.; Choi, J.-Y.; Park, M. H.; Yang, C. W.; Pribat, D.; Lee, Y. H. Synthesis of Large-Area Graphene Layers on Poly-Nickel Substrate by Chemical Vapor Deposition: Wrinkle Formation. *Adv. Mater.* **2009**, *21*, 2328−2333.

DOI: 10.1021/acsami.8b19372
ACS Appl. Mater. Interfaces 2019, 11, 11645−11653

(28) Sun, Z.; Yan, Z.; Yao, J.; Beitler, E.; Zhu, Y.; Tour, J. M. Growth of Graphene from Solid Carbon Sources. *Nature* **2010**, *468*, 549−552.
(29) Li, X.; Cai, W.; An, J.; Kim, S.; Nah, J.; Yang, D.; Piner, R.; Velamakanni, A.; Jung, I.; Tutuc, E.; Banerjee, S. K.; Colombo, L.; Ruoff, R. S. Large-Area Synthesis of High-Quality and Uniform Graphene Films on Copper Foils. *Science* **2009**, *324*, 1312−1314.
(30) Kim, K. S.; Zhao, Y.; Jang, H.; Lee, S. Y.; Kim, J. M.; Kim, K. S.; Ahn, J.-H.; Kim, P.; Choi, J.-Y.; Hong, B. H. Large-Scale Pattern Growth of Graphene Films for Stretchable Transparent Electrodes. *Nature* **2009**, *457*, 706−710.
(31) Jo, G.; Choe, M.; Cho, C.-Y.; Kim, J. H.; Park, W.; Lee, S.; Hong, W.-K.; Kim, T.-W.; Park, S.-J.; Hong, B. H.; Kahng, Y. H.; Lee, T. Large-Scale Patterned Multi-Layer Graphene Films as Transparent Conducting Electrodes for GaN Light-Emitting Diodes. *Nanotechnology* **2010**, *21*, 175201.
(32) Jang, Y.; Kwon, S.-J.; Shin, J.; Jeong, H.; Hwang, W.-T.; Kim, J.; Koo, J.; Ko, T. Y.; Ryu, S.; Wang, G.; Lee, T.-W.; Lee, T. Interface-Engineered Charge-Transport Properties in Benzenedithiol Molecular Electronic Junctions via Chemically p-Doped Graphene Electrodes. *ACS Appl. Mater. Interfaces* **2017**, *9*, 42043−42049.
(33) Kim, J.; Jeong, H.; Seong, S.; Kim, M.; Kim, D.; Hwang, W.-T.; Jang, Y.; Choi, B. Y.; Koo, J.; Park, S. B.; Noh, J.; Lee, T. Comparative Study for Electrical Transport Characteristics of Self-Assembled Monolayers Formed by Benzenethiol, Cyclohexanethiol, and Adamantanethiol. *Curr. Appl. Phys.* **2017**, *17*, 1459−1464.
(34) Snegir, S.; Mukha, I.; Sysoiev, D.; Lacaze, E.; Huhn, T.; Pluchery, O. Optically controlled properties of nanoparticles stabilised by photochromic difurylethene-base diarylethenes. *Materialwiss. Werkstofftech.* **2016**, *47*, 229−236.
(35) Cho, C.-Y.; Choe, M.; Lee, S.-J.; Hong, S.-H.; Lee, T.; Lim, W.; Kim, S.-T.; Park, S.-J. Near-Ultraviolet Light-Emitting Diodes with Transparent Conducting Layer of Gold-Doped Multi-Layer Graphene. *J. Appl. Phys.* **2013**, *113*, 113102.
(36) Kim, T.-W.; Wang, G.; Lee, H.; Lee, T. Statistical Analysis of Electronic Properties of Alkanethiols in Metal-Molecule-Metal Junctions. *Nanotechnology* **2007**, *18*, 315204.
(37) Higashiguchi, K.; Matsuda, K.; Kobatake, S.; Yamada, T.; Kawai, T.; Irie, M. Fatigue Mechanism of Photochromic 1,2-Bis(2,5-dimethyl-3-thienyl)perfluorocyclopentene. *Bull. Chem. Soc. Jpn.* **2000**, *73*, 2389−2394.
(38) Kim, Y.; Hellmuth, T. J.; Sysoiev, D.; Pauly, F.; Pietsch, T.; Wolf, J.; Erbe, A.; Huhn, T.; Groth, U.; Steiner, U. E.; Scheer, E. Charge Transport Characteristics of Diarylethene Photoswitching Single-Molecule Junctions. *Nano Lett.* **2012**, *12*, 3736−3742.
(39) Selzer, Y.; Cai, L.; Cabassi, M. A.; Yao, Y.; Tour, J. M.; Mayer, T. S.; Allara, D. L. Effect of Local Environment on Molecular Conduction: Isolated Molecule versus Self-Assembled Monolayer. *Nano Lett.* **2005**, *5*, 61−65.
(40) Li, B.; Famili, M.; Pensa, E.; Grace, I.; Long, N. J.; Lambert, C.; Albrecht, T.; Cohen, L. F. Cross-plane Conductance through a Graphene/Molecular Monolayer/Au Sandwich. *Nanoscale* **2018**, *10*, 19791−19798.
(41) Liu, N.; Pan, Z.; Fu, L.; Zhang, C.; Dai, B.; Liu, Z. The Origin of Wrinkles on Transferred Graphene. *Nano Res.* **2011**, *4*, 996−1004.
(42) Chen, X.; Zhang, L.; Chen, S. Large Area CVD Growth of Graphene. *Synth. Met.* **2015**, *210*, 95−108.
(43) Jeong, H.; Hwang, W.-T.; Kim, P.; Kim, D.; Jang, Y.; Min, M.; Xiang, D.; Song, H.; Park, Y. D.; Jeong, H.; Lee, T. Investigation of Inelastic Electron Tunneling Spectra of Metal-Molecule-Metal Junctions Fabricated Using Direct Metal Transfer Method. *Appl. Phys. Lett.* **2015**, *106*, 063110.
(44) Yuan, L.; Jiang, L.; Zhang, B.; Nijhuis, C. A. Dependency of the Tunneling Decay Coefficient in Molecular Tunneling Junctions on the Topography of the Bottom Electrodes. *Angew. Chem., Int. Ed.* **2014**, *53*, 3377−3381.
(45) Scheer, E.; Cuevas, J. C. *Molecular Electronics: An Introduction to Theory and Experiment*; World Scientific, 2010; Chapter 13, pp 364−366.
(46) Briechle, B. M.; Kim, Y.; Ehrenreich, P.; Erbe, A.; Sysoiev, D.; Huhn, T.; Groth, U.; Scheer, E. Current-voltage characteristics of single-molecule diarylethene junctions measured with adjustable gold electrodes in solution. *Beilstein J. Nanotechnol.* **2012**, *3*, 798−808.
(47) Moth-Poulsen, K.; Bjørnholm, T. Molecular Electronics with Single Molecules in Solid-State Devices. *Nat. Nanotechnol.* **2009**, *4*, 551−556.
(48) Yuan, L.; Nerngchamnong, N.; Cao, L.; Hamoudi, H.; Del Barco, E.; Roemer, M.; Sriramula, R. K.; Thompson, D.; Nijhuis, C. A. Controlling the Direction of Rectification in a Molecular Diode. *Nat. Commun.* **2015**, *6*, 6324.
(49) TURBOMOLE V7.3; a development of University of Karlsruhe and Forschungszentrum Karlsruhe GmbH, 1989−2007; TURBOMOLE GmbH, since 2007; available from http://www.turbomole.com.
(50) Perdew, J. P.; Wang, Y. Accurate and Simple Analytic Representation of the Electron-Gas Correlation Energy. *Phys. Rev. B: Condens. Matter Mater. Phys.* **1992**, *45*, 13244−13249.
(51) Perdew, J. P.; Burke, K.; Wang, Y. Generalized Gradient Approximation for the Exchange-Correlation Hole of a Many-Electron System. *Phys. Rev. B: Condens. Matter Mater. Phys.* **1996**, *54*, 16533−16539.
(52) Perdew, J. P.; Burke, K.; Ernzerhof, M. Generalized Gradient Approximation Made Simple. *Phys. Rev. Lett.* **1996**, *77*, 3865−3868.
(53) Martin, R. M. *Electronic Structure: Basic Theory and Practical Methods*; Cambridge University Press, 2004.
(54) van Setten, M. J.; Weigend, F.; Evers, F. The GW-Method for Quantum Chemistry Applications: Theory and Implementation. *J. Chem. Theory Comput.* **2012**, *9*, 232−246.
(55) Kaplan, F.; Harding, M. E.; Seiler, C.; Weigend, F.; Evers, F.; van Setten, M. J. Quasi-Particle Self-Consistent GW for Molecules. *J. Chem. Theory Comput.* **2016**, *12*, 2528−2541.
(56) Comstock, M. J.; Levy, N.; Kirakosian, A.; Cho, J.; Lauterwasser, F.; Harvey, J. H.; Strubbe, D. A.; Fréchet, J. M. J.; Trauner, D.; Louie, S. G.; Crommie, M. F. Reversible Photomechanical Switching of Individual Engineered Molecules at a Metallic Surface. *Phys. Rev. Lett.* **2007**, *99*, 038301.
(57) Gahl, C.; Schmidt, R.; Brete, D.; McNellis, E. R.; Freyer, W.; Carley, R.; Reuter, K.; Weinelt, M. Structure and Excitonic Coupling in Self-Assembled Monolayers of Azobenzene-Functionalized Alkanethiols. *J. Am. Chem. Soc.* **2010**, *132*, 1831−1838.

DOI: 10.1021/acsami.8b19372
ACS Appl. Mater. Interfaces 2019, 11, 11645−11653